

Supplementary Data

Supplementary Methods

Preconjugation of adhesion peptides to poly(ethylene glycol)

Norbornene-functionalized poly(ethylene glycol) (PEGNB, 20 kDa, 8-arm; Jenkem) was dissolved in H₂O at a 0.01 mM concentration and combined with 0.05% w/v Irgacure 2959 photoinitiator (I2959; Ciba Specialty Chemicals, Tarrytown, NY) as well as a 2× molar excess of either head-to-tail cyclized Arg-Gly-Asp-[d-Phe]-Cys (cyclic RGD; Genscript, Piscataway, NJ) adhesion peptide or linear H-Cys-Arg-Gly-Asp-Ser-NH₂ (linear RGD, Genscript). The mixtures were reacted under 365 nm ultraviolet (UV) light for 5 minutes at a dose rate of 4.5 mW/cm² to covalently attach the peptides to norbornene groups through the thiol-ene reaction.^{S1}

To remove buffer salts and unreacted peptides from the decorated PEGNB, the reaction mixtures were dialyzed in deionized H₂O for 2 days. The dialyzed solutions were frozen in liquid nitrogen and lyophilized. The coupling efficiency of peptides to the PEGNB was quantified using proton nuclear magnetic resonance (NMR) to detect disappearances of alkene protons at 6.8–7.2 PPM caused by covalent bonding of the peptides to the norbornene group.

Preparation of poly(ethylene glycol) hydrogel solutions

Proangiogenic hydrogels consisted of PEGNB molecules, preconjugated PEGNB-RGD molecules, MMP-degradable H-Lys-Cys-Gly-Gly-Pro-Gln-Gly-Ile-Trp-Gly-Gln-Gly-Cys-Lys-NH₂ crosslinking peptide (MMPDP; Genscript), and 0.2% w/v I2959 photoinitiator (Ciba, Basel, Switzerland) dissolved in phosphate-buffered saline (1× PBS) (Fig. 1B). Before inclusion in precursor solutions, the purity of the crosslinking peptide was verified using Ellman's Assay (Thermo Fisher). Crosslinking molecules were added to the solution to achieve crosslinking of 50% total norbornene functional groups present in solution. Once completed, all hydrogel solutions were immediately stored at –80°C, thawed immediately before use, and subjected to only one freeze–thaw cycle before use.

Assembling hydrogel arrays

Hydrogel screening arrays were constructed as follows: μ -plate angiogenesis 96-well plates (Ibidi, USA, Madison

WI) were coated using poly(L-lysine) (PLL; 150,000–300,000 Da; Sigma-Aldrich). A 0.01% v/v solution of PLL in H₂O was pipetted into the wells at 10 μ L volume to evenly coat the bottoms of the wells. After a 5-minute incubation at room temperature, the solution was aspirated from all wells. Each well was then washed with H₂O twice before drying.

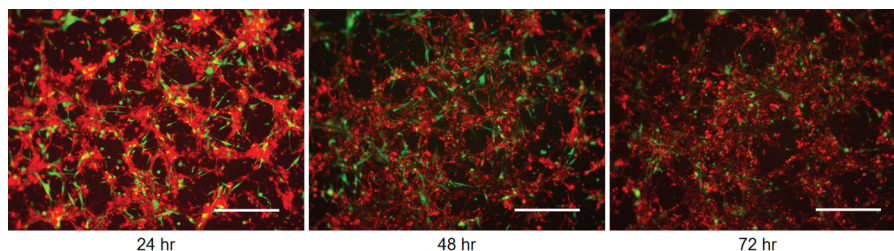
Poly(ethylene glycol) (PEG) hydrogel solutions were pipetted into the wells in 9 μ L volumes and cured for 8 minutes under 365 nm, 4.5 mW/cm² UV light. Afterward, the hydrogels were swollen at 2°C–8°C in 70 μ L 1× PBS overnight. In case of Matrigel™ arrays, growth factor-reduced Geltrex® (Thermo Fisher) was added to the 96-well angiogenesis plates in 10 μ L volumes and incubated in a humidified 37°C incubator for at least 30 minutes before cell seeding (Fig. 1).

Verifying effects of receptor tyrosine kinase signaling inhibition and oxidative stress on neurovascular unit morphology

Using cell culture conditions and neurovascular unit (NVU) coculture ratios determined previously, a 0.2–40 μ M dose range of sunitinib malate, a receptor tyrosine kinase inhibitor affecting multiple angiogenic signaling pathways,^{S2} and a 0.03–4 mM dose range of hydrogen peroxide, a direct inducer of oxidative stress,^{S3,S4} were applied to the NVU model to verify morphological changes to capillary network formation.

The three cell types of the NVU model were passaged, for simultaneous seeding onto the PEG hydrogels. The endothelial cells (ECs) were stained using Cell Tracker Red, and either pericytes (PCs) or astrocytes (ACs) were stained using Cell Tracker Green, but not both cell types simultaneously. Endothelial maintenance medium was combined with either 0.2% v/v dimethyl sulfoxide (DMSO) or DMSO and inhibitors at double the desired final concentrations and added as 35 μ L volumes to each well (e.g., a culture well assigned to a 10 μ M sunitinib malate condition was given 35 μ L of 20 μ M sunitinib malate in medium). All conditions contained 0.2% v/v DMSO to maintain equivalent concentration of vehicle throughout the experiment. Afterward, 35 μ L endothelial maintenance medium containing 22,500 ECs, 1125 PCs, and 2183 ACs were added to each well of the hydrogel array.

Cells were left undisturbed for 24 hours, after which the NVU networks were photographed by epifluorescence



SUPPLEMENTARY FIG. S1. The NVU model cultured for 72 hours. Medium was exchanged in the wells after 24 and 72 hours of culture. Red: ECs. Green: ACs. Scale bar: 0.5 mm.

microscopy using a Nikon Eclipse microscope. After photography, cells were fixed by 30-minute incubation in 10% buffered formalin.

Cytotoxicity studies

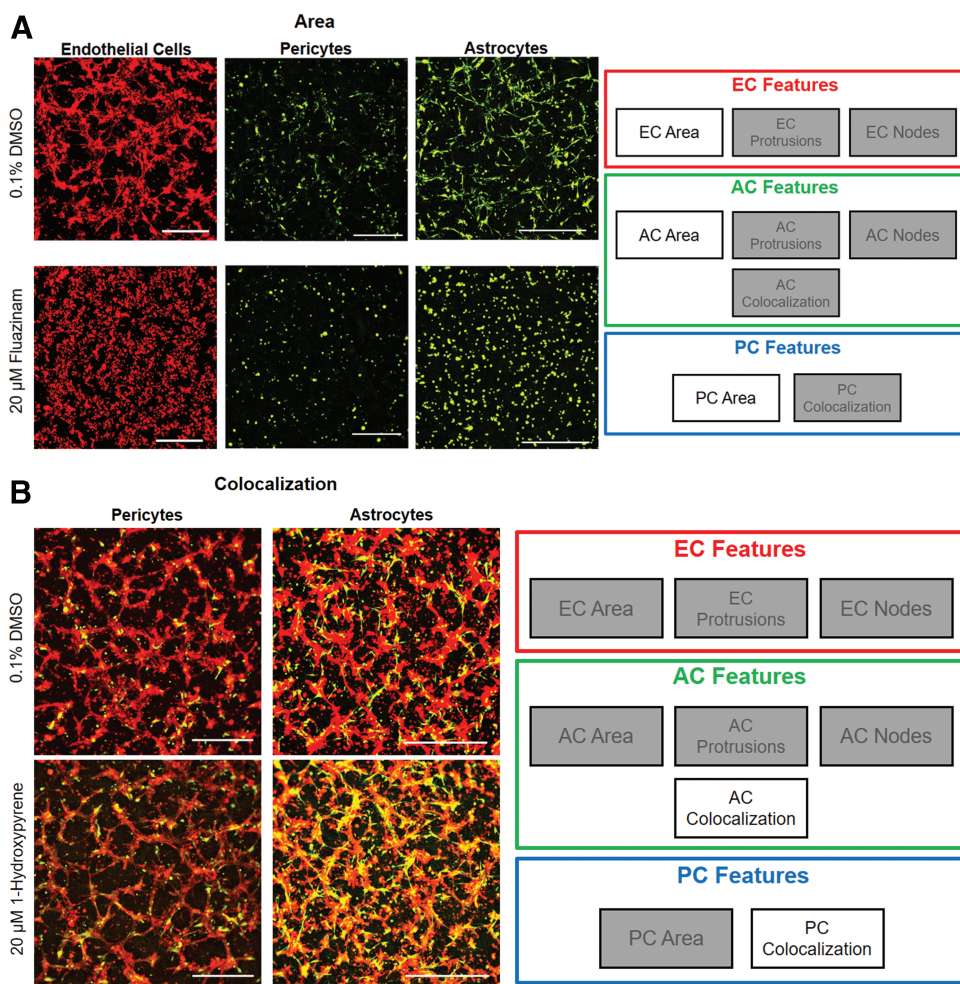
Cytotoxicity studies were carried out according to the Cytotox 96[®] Non-Radioactive Cytotoxicity Assay kit and protocol (Promega, Fitchburg, WI). The assay kit detects activity of alcohol dehydrogenase released into medium after cell death by necrosis. NVU models were seeded onto PEG hydrogel arrays without cell tracker staining, along with all critical priority chemicals, and incubated at 37°C for 3.75 hours. The dose application range used for each chemical was identical to those used in dose–response curve generation. Afterward, 7 μ L lysis buffer was added into preassigned lysis buffer control wells. After a further 45-minute incubation (4.5-hour incubation total), 50 μ L cell culture medium was removed from each well and tested for lactate dehydrogenase (LDH) activity using the cytotoxicity kit. The chemical incubation time was 4.5 hours to measure LDH activity

before the 9-hour half-life of LDH in medium, as recommended by the manufacturer protocol (Promega). A control of lysis buffer (included in CytoTox[®] Assay; Promega) represented 100% cytotoxicity. The NVU models themselves were fixed by 30-minute incubation in 10% buffered formalin.

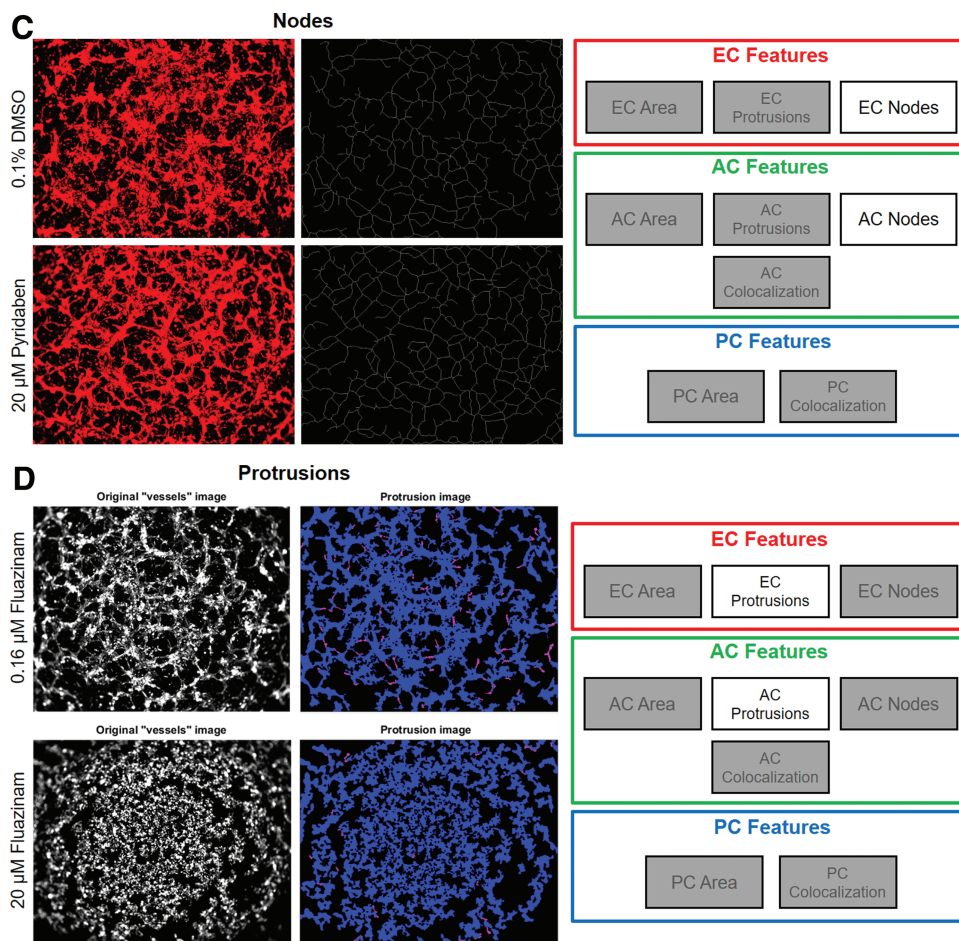
Supplementary Results

Receptor tyrosine kinase inhibition and oxidative stress on coculture model

The NVU model was incubated with sunitinib malate and hydrogen peroxide to confirm that significant chemically mediated changes to network morphology were detectable and quantifiable. Sunitinib malate and hydrogen peroxide disrupt network formation through inhibition of receptor tyrosine kinase signaling^{S2} and increased oxidative stress,^{S3,S4} respectively. Incubation with sunitinib malate resulted in disrupted network formation and cell clustering. Incubation with hydrogen peroxide resulted in rounded nonadhesive cells gathering toward the centers of the



SUPPLEMENTARY FIG. S2. Morphological analysis of NVU features, readouts sorted by relevance to ECs, ACs, and PCs behavior. (A) Endothelial Network Area, Astrocyte Area, and Pericyte Area with and without fluazinam treatment on PEG hydrogels. (B) Colocalization of PCs and ACs with EC networks. (C) Network organization quantified as the number of branching intersections in skeletonized network images. (D) Total area of fine bridges and protrusions in binary images. ACs, astrocytes; ECs, endothelial cells; NVU, neurovascular unit; PCs, pericytes; PEG, poly(ethylene glycol).



SUPPLEMENTARY FIG. S2. (Continued).

wells (Supplementary Fig. S3A). In the case of Sunitinib Malate treatment, the effects on endothelial network area, protrusions, and nodes were only clearly quantifiable at a 40 μ M dose rather than at lower doses (Supplementary Fig. S3B). In contrast, hydrogen peroxide affected endothelial network area and protrusions in a gradual dose-dependent manner (Supplementary Fig. S3C), although the node measurement was not suitable for quantifying morphologies of cells concentrated at the centers of NVU model wells.

Cytotoxic effects of critical priority chemicals

To determine whether morphological effects on the NVU were the result of necrosis and immediate cell membrane permeabilization by any applied chemicals, we utilized a cytotoxicity assay to detect activity by LDH released into medium upon chemical dosing. We observed low levels of cytotoxicity associated with most of the chemical treatments performed here, with most of the significant increases observed at the highest dosage levels of chemicals applied. The only exception was 5HPP33, which exhibited increased cytotoxicity levels at 20 μ M concentrations. However, the active concentration 50 (AC₅₀) values generated with 5HPP33 exposure were observed at 2–4 μ M doses, well below the 20 μ M dose.

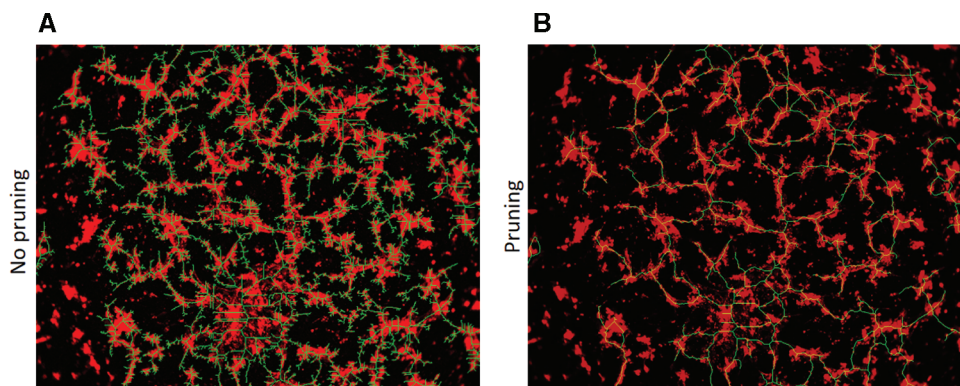
In most of the cases wherein increases in cytotoxicity were significant, percentage cytotoxicity did not exceed 30%, indi-

cating that in most cases, chemical dosing did not result in high levels of cytotoxicity. The only cases wherein cytotoxicity increased beyond 30% were cases such as 4-Nonylphenol Branched, 5HPP33, reserpine and 1-hydroxypyrene (Supplementary Fig. S6). A control of lysis buffer (included in Cytotox Assay) represented 100% cytotoxicity.

Supplementary Discussion

The most common outcome of chemical treatment observed in these studies was the adoption of rounded nonadhesive morphology, which is likely associated with increased oxidative stress and apoptosis. The role of oxidative stress in inducing this outcome was confirmed using NVU incubation with hydrogen peroxide, which induces increased oxidative stress in cells directly^{S3,S4} (Supplementary Fig. S3).

Phenolphthalein, disulfiram, triclocarban, fluazinanam, 1-hydroxypyrene, and 5HPP33 all triggered this morphological outcome. However, the underlying mechanisms of action are suspected to be different for each chemical. For example, phenolphthalein can interfere with estrogen receptor α signaling to result in increased BMP6 expression and subsequent increases in oxidative stress.^{S5-S7} Disulfiram, an inhibitor of alcohol dehydrogenases, may inhibit activity of PLK-1 and make cells more susceptible to apoptosis.^{S8} Finally, triclocarban, an antibacterial agent, can interfere



SUPPLEMENTARY FIG. S3. Pruning skeletonized network images to remove processing artifacts. (A) Skeletonized image without pruning. (B) Overall form of the skeletonized image remains intact, but small extraneous branches were removed using an automated function.

with the expression of antioxidant enzymes, particularly glutathione,^{S9,S10} and also results in increased oxidative stress.

These suspected mechanisms require further adverse outcome pathway development for confirmation, as the morphological outcomes alone do little to inform experimenters on divergent pathways, leading to the same apoptotic outcome. 5HPP33, synthetic variant of thalidomide, induced a similar morphological change to the aforementioned chemicals. Rather than affecting oxidative stress, it inhibits microtubule formation in ECs and, therefore, inhibits angiogenesis and tissue growth.^{S11–S13} The distinguishing property of 5HPP33 was that it generated usable AC_{50} values of eight of nine morphological characteristics measured here. This may be a unique outcome of microtubule inhibition. 1-Hydroxypyrene, another chemical that resulted in rounded nonadhesive cell morphology, required very high doses (maximum dose $160\ \mu\text{M}$) to generate reliable AC_{50} values compared with other chemicals requiring doses of $80\ \mu\text{M}$ or less. Given that 1-hydroxypyrene is a common metabolite present in low concentrations in patients exposed to air pollution and smoking,^{S14} it may require extreme concentrations of the metabolite to disrupt the neurovascular function. This prediction is supported by the fact that 1-hydroxypyrene demonstrated significantly elevated cytotoxicity at its maximum doses.

When considering the chemical structures of phenolphthalein, disulfiram, triclocarban, fluazinam, 1-hydroxypyrene, and 5HPP33, a common feature of these molecules is the ability to maintain charged chemical groups on aromatic rings.^{S15} The only exception to this is disulfiram, which is essentially two thiocarbamide groups bridged by a disulfide bond. 5HPP-33, the most potent member of this group, resembles a hormone in addition to its ability to maintain an aromatic phenol group.

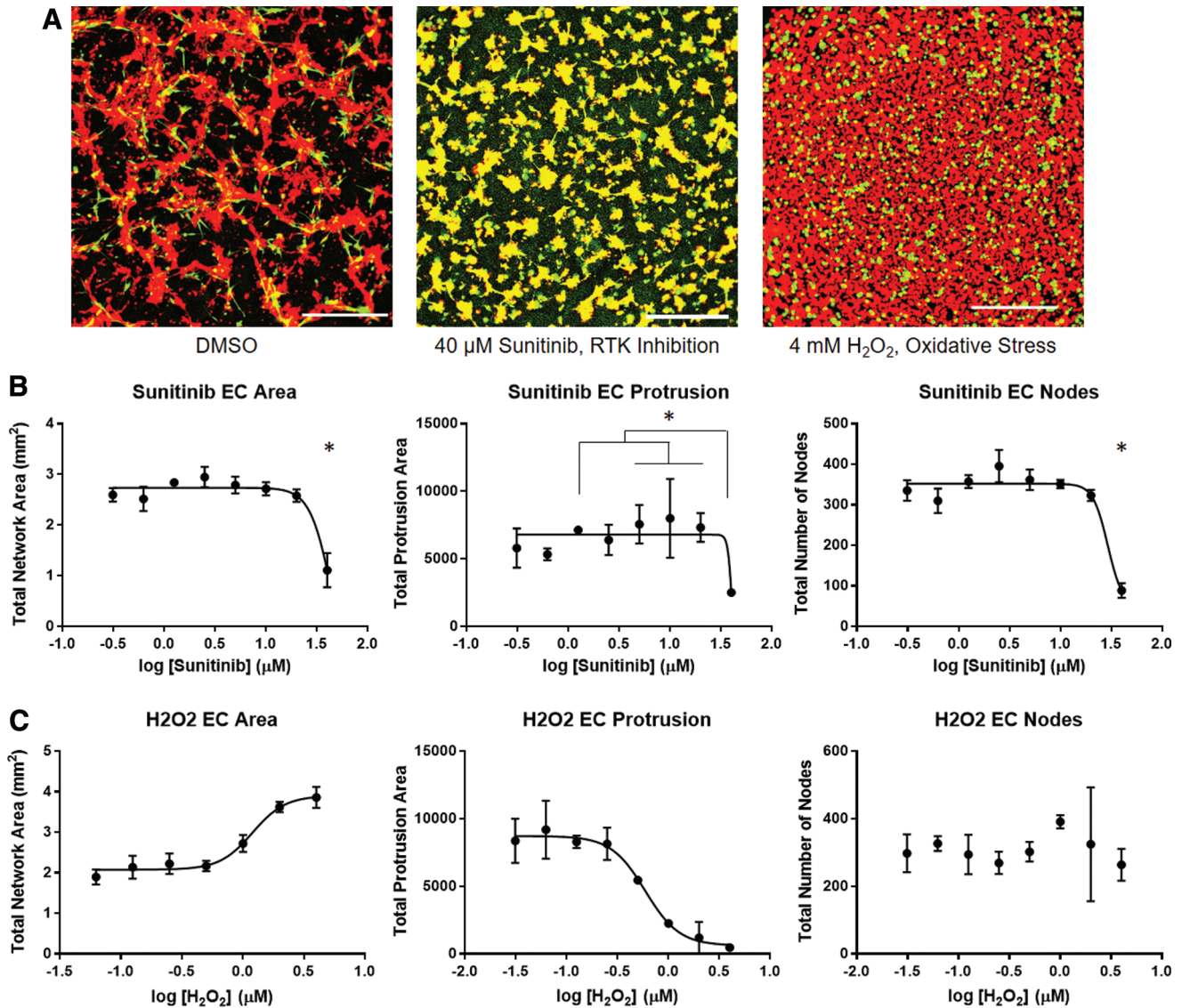
We were able to observe an instance where oxidative stress would lead to two distinct morphological outcomes depending on whether apoptotic pathways were activated or not. In this study, pyridaben, a pesticide that interferes with mitochondrial complex 1 and the electron transport chain,^{S16,S17} was the only chemical that brought about the formation of densely meshed fine capillary networks in the

PEG-based NVU model. This outcome may conceivably be linked to changes in the electron transport chain. In contrast, fluazinam, a fungicide, also interferes with oxidative respiration in cells. However, in addition to mitochondrial complex 1, fluazinam is also known to affect p38 and p53 activity,^{S18,S19} and, therefore, leads to increased oxidative stress and apoptosis. Therefore, fluazinam resulted in NVU cells adopting rounded nonadhesive morphologies similar to phenolphthalein, disulfiram, and triclocarban.

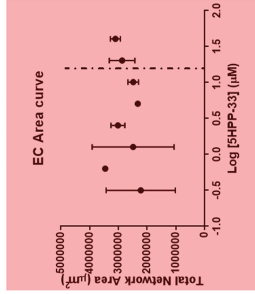
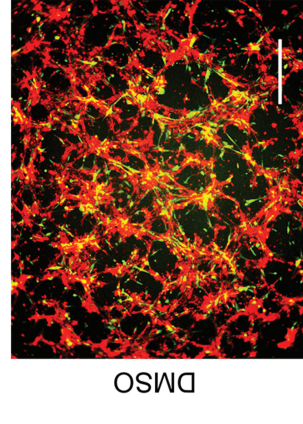
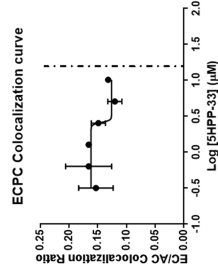
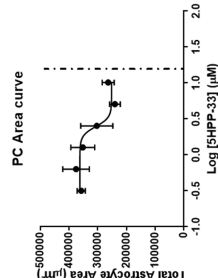
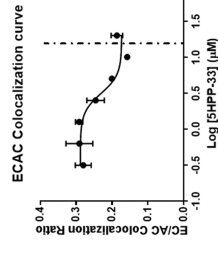
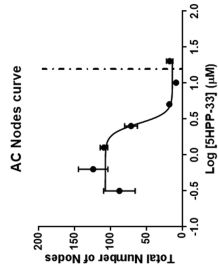
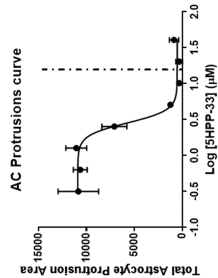
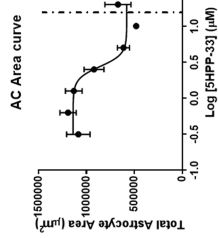
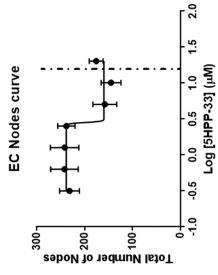
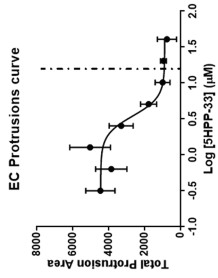
When considering the chemical structures of pyridaben and fluazinam, these chemicals similarly feature pairs of ring structures containing multiple charged groups. The presence of charged groups on fluazinam is greater than that on pyridaben, with fluazinam containing tetrafluoro groups where pyridaben contains tert-butyl groups, among other differences.^{S20} This may be related to fluazinam's functionality in causing oxidative stress in addition to affecting the electron transport chain. If these morphologies can suggest general categories of pathways for further investigation, we expect this technology to accelerate the process of deriving safe exposure limits based on phenotypic changes in human tissue.

We observed that several chemicals were highly effective at generating AC_{50} values in both Matrigel and PEG-based NVU models, whereas other chemicals were only effective in one or neither model. We predict that comparing the performance between the two NVU models may highlight whether different models are amenable to detecting specific mechanisms of action over others.

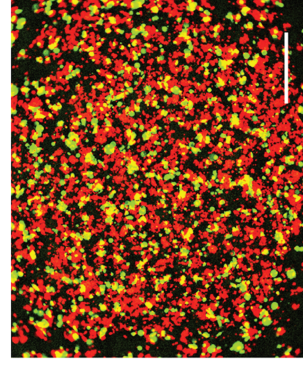
5HPP33 was almost universally effective at generating usable AC_{50} values in both PEG-based and Matrigel-based models. This may suggest that the effects of microtubule inhibition may be highly visible on Matrigel and PEG-based models. Disulfiram was also similarly effective on both models, though never as effective as 5HPP33. When considering the chemical structures of these molecules, a common feature is the presence of short carbon chains^{S20} that may interfere with chemical–extracellular matrix interactions. Other chemicals related to oxidative stress—fluazinam, phenolphthalein, and triclocarban—generated fewer usable AC_{50} values on Matrigel than on PEG-based NVU models.



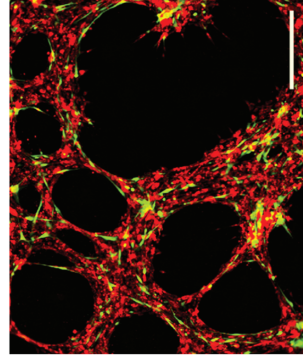
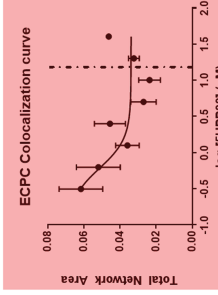
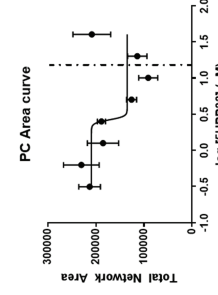
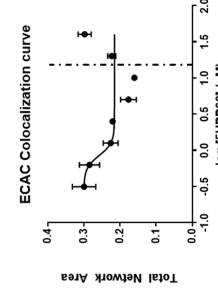
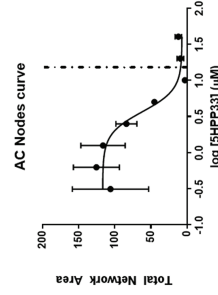
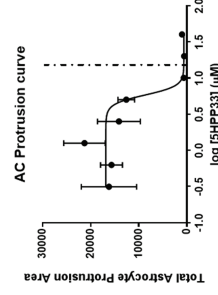
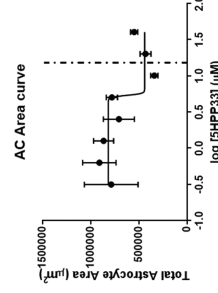
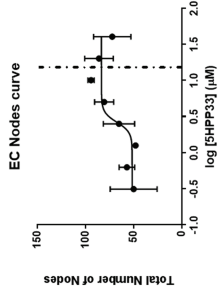
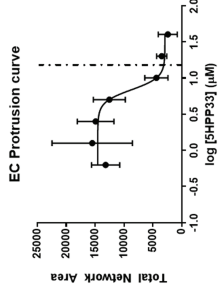
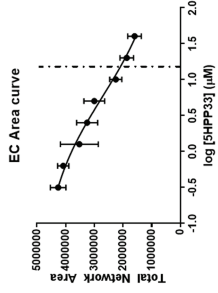
SUPPLEMENTARY FIG. S4. NVU model response to sunitinib malate and hydrogen peroxide treatment. **(A)** Representative examples of morphological differences between DMSO-treated NVU models and those treated with either 40 μM sunitinib malate or 4 mM hydrogen peroxide. Sunitinib malate treatment resulted in the formation of disconnected structures throughout the wells, whereas hydrogen peroxide resulted in a large aggregate of nonadhesive cells forming at the centers of each well. Scale bar: 0.5 mm. Red: ECs. Green: ACs. **(B)** Endothelial morphology parameters quantified with varying doses of sunitinib malate. Forty micromolar doses of sunitinib malate caused significant changes in NVU morphology compared with those observed in lower doses. $*p < 0.05$, Tukey's multiple comparisons test. A single * denotes significant differences compared with all other sunitinib malate doses. **(C)** Endothelial morphology parameters quantified with varying doses of hydrogen peroxide. Gradual dose-dependent changes to NVU morphology, with exception to the nodes measurement, were observed with hydrogen peroxide treatment. DMSO, dimethyl sulfoxide.

A**5HPP33, PEG Hydrogel**

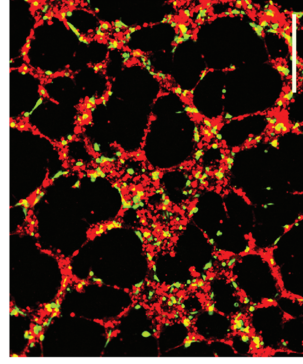
DMSO



40 µM 5HPP-33

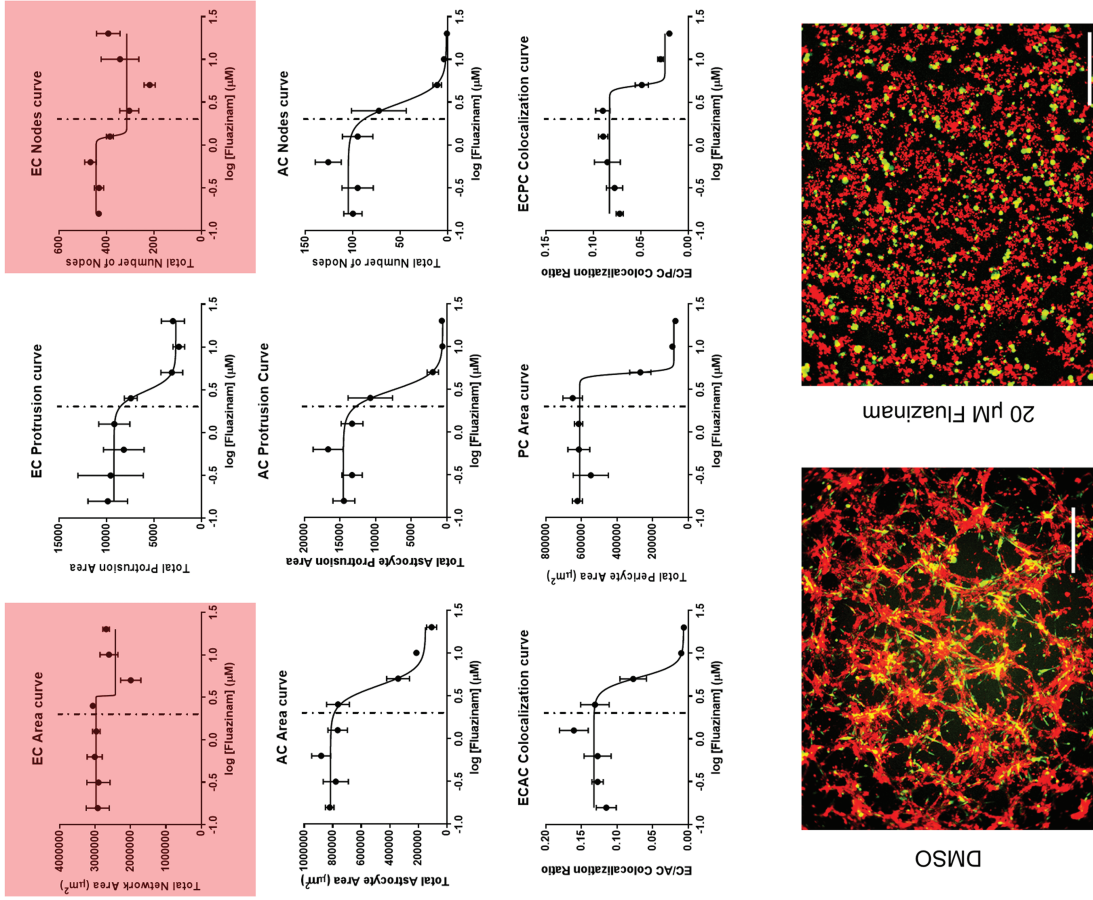
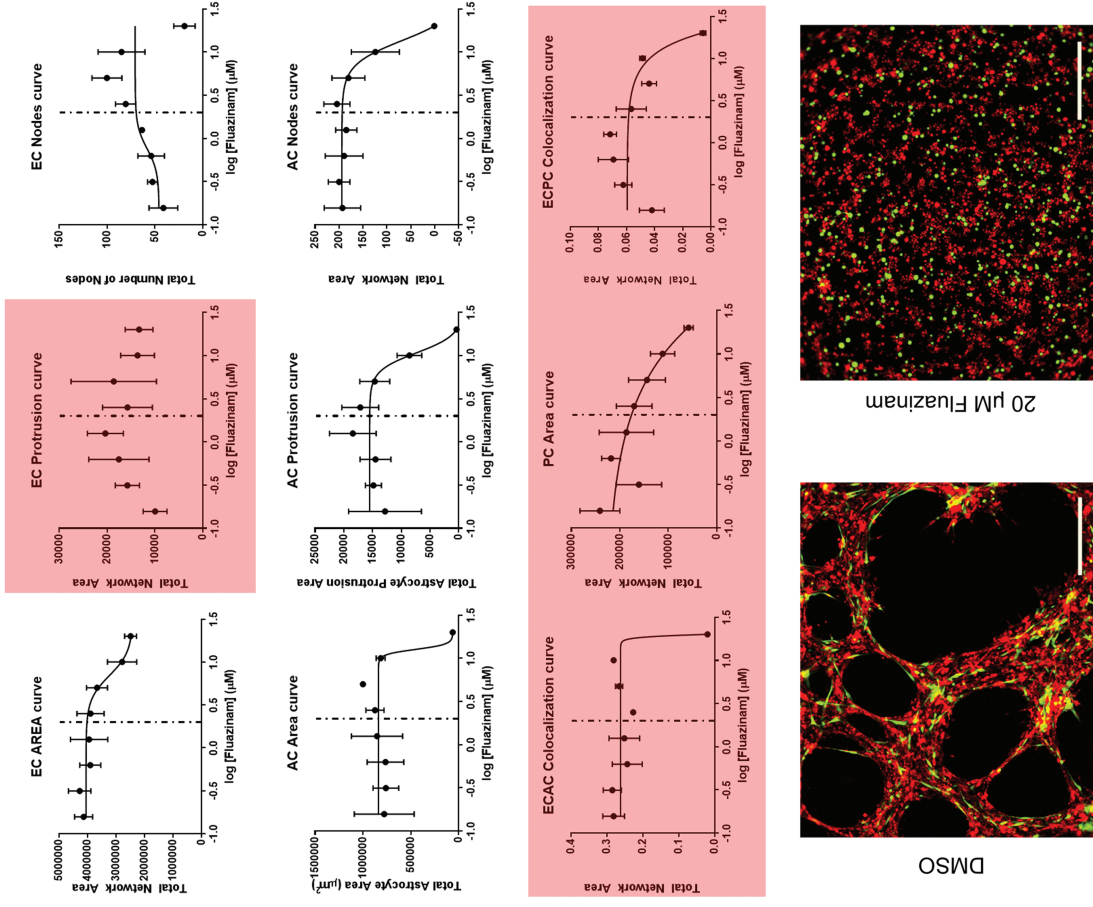
5HPP33, Matrigel

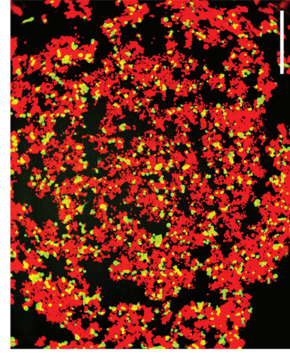
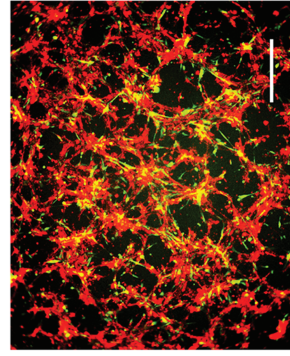
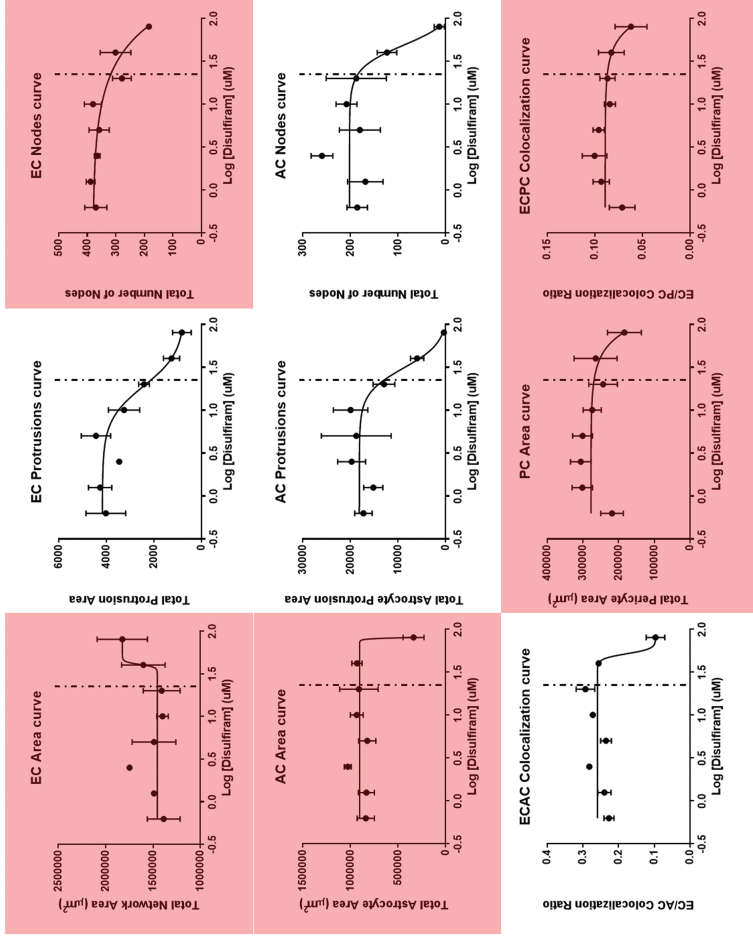
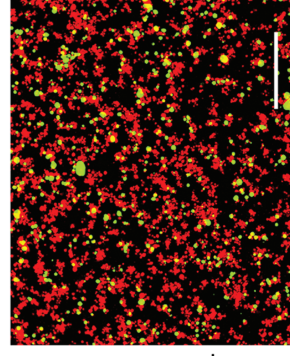
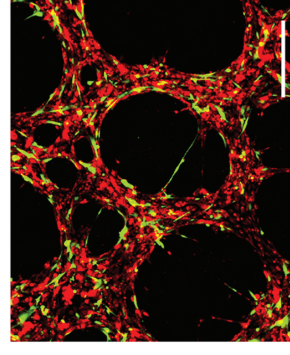
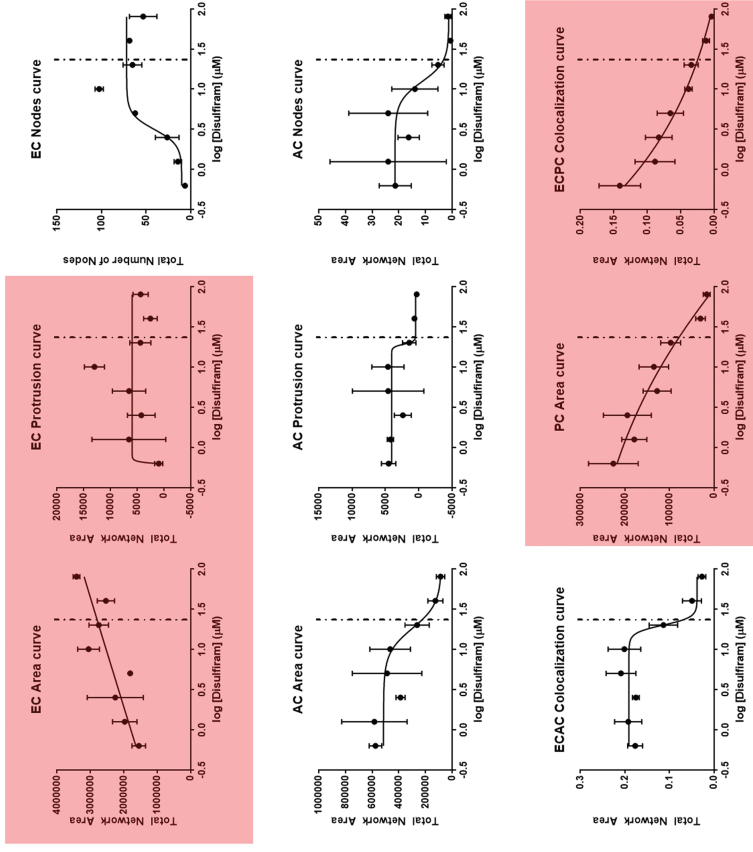
DMSO



40 µM 5HPP-33

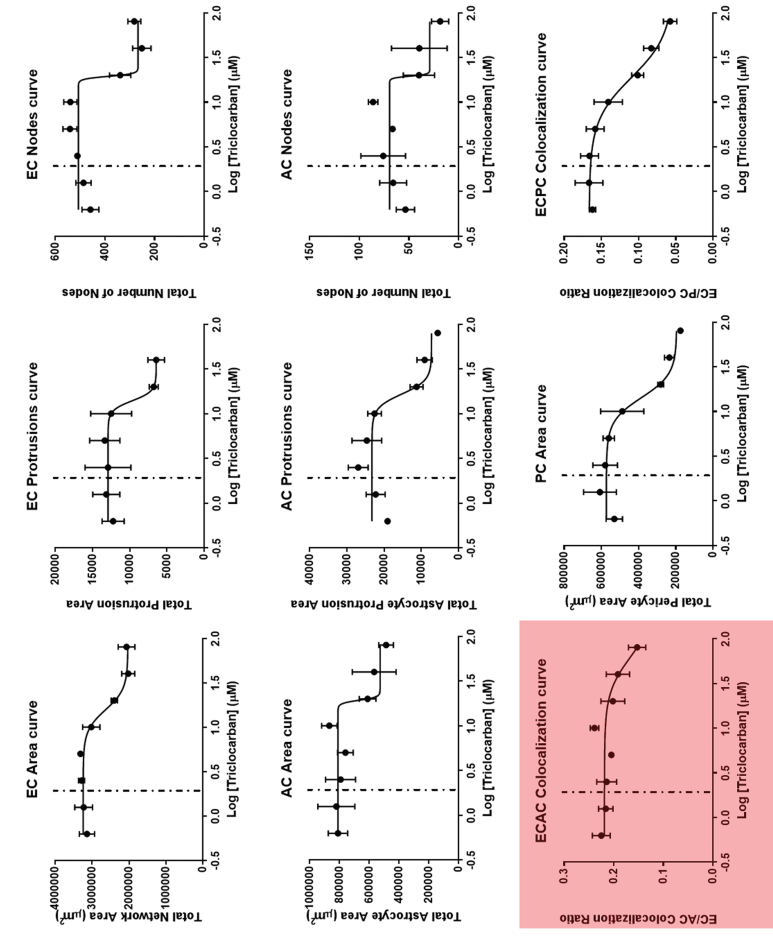
SUPPLEMENTARY FIG. S5. Representative graphs of all network morphology parameters, and representative images of NVU networks under DMSO control and maximal chemical doses. Dose-response curves overlaid in red represent morphological measurements that failed to generate consistent AC_{50} values or trends over multiple technical replicates, failed to generate usable AC_{50} values within the range of doses tested, or failed to converge into sigmoidal curves. Dose-response curves overlaid in blue represent situations wherein chemical autofluorescence interfered with the measurement. Red: ECs. Green: ACs. Scale bar: 0.5 mm. Dotted line: median AC_{50} value from ToxCast forecaster database, assays on human vascular cells. **(A)** 5HPP-33. **(B)** Fluzazinam. **(C)** Disulfiram. **(D)** Trilocarban. **(E)** Phenolphthalein. **(F)** 1-Hydroxyxyrene. **(G)** Pyridaben. **(H)** Reserpine. **(I)** 4 Nonylphenol, Branched. **(J)** Quercetin. AC_{50} , active concentration 50.

B**Fluazinam, PEG Hydrogel****Fluazinam, Matrigel****SUPPLEMENTARY FIG. S5.** (Continued).

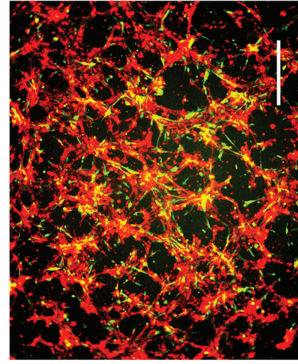
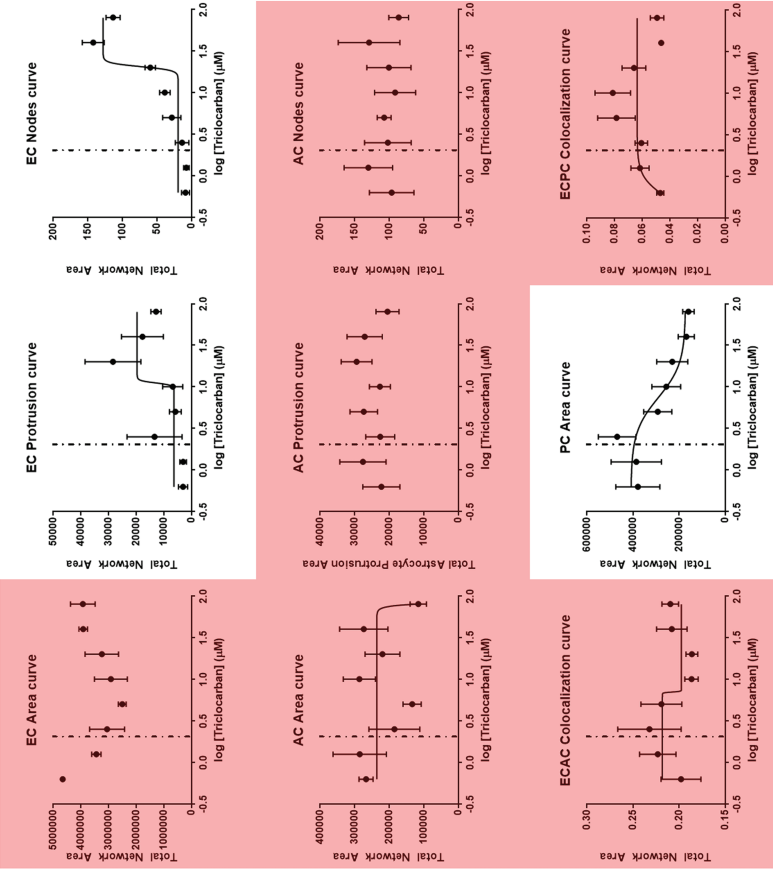
C**Disulfiram, PEG Hydrogel****Disulfiram, Matrigel****SUPPLEMENTARY FIG. S5.** (Continued).

D

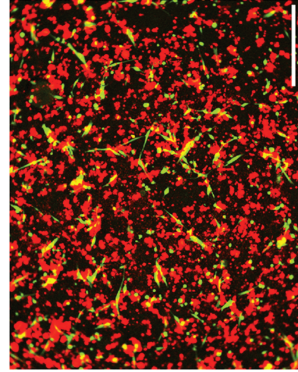
Triclocarban, PEG Hydrogel



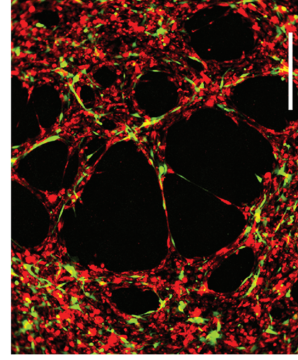
Triclocarban, Matrigel



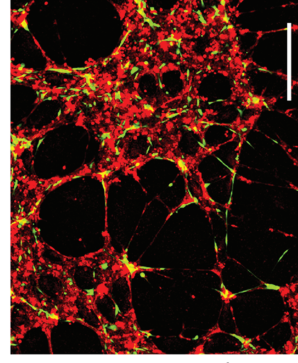
DMSO



80 μ M Triclocarban



DMSO

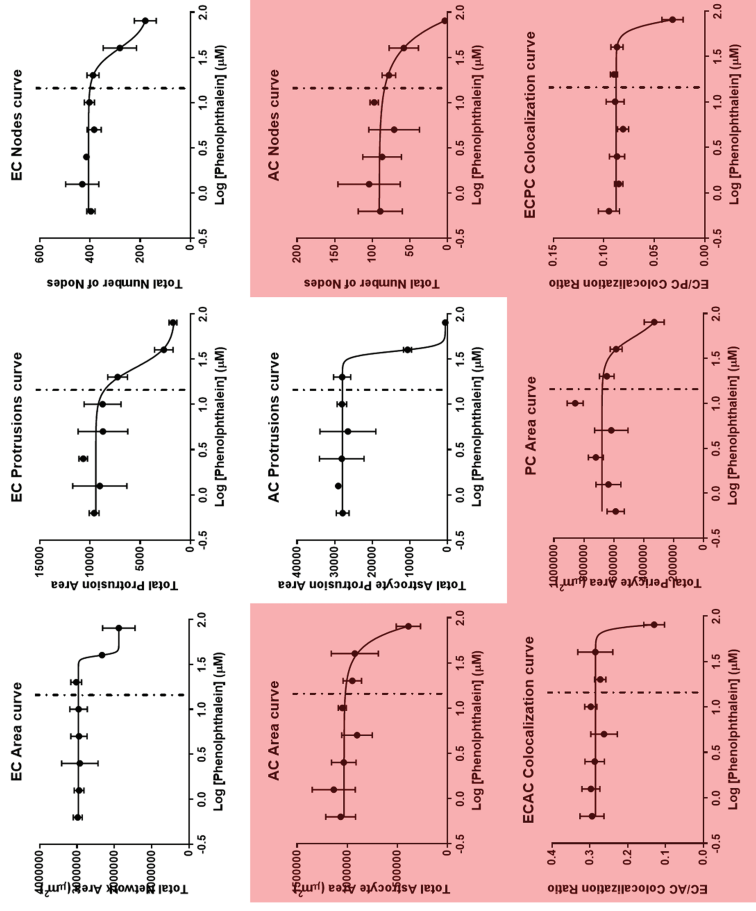


80 μ M Triclocarban

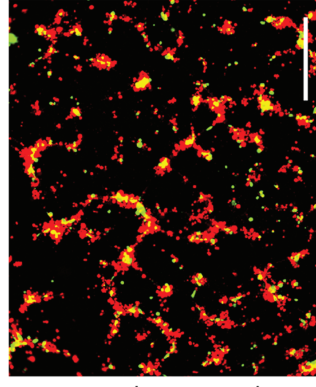
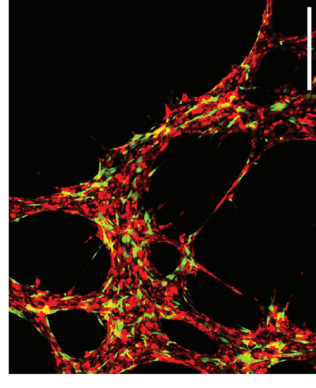
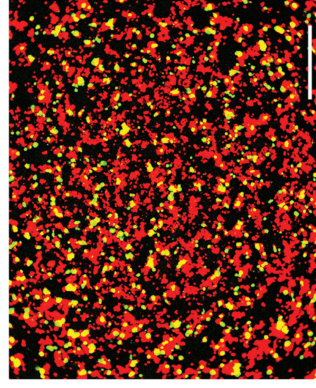
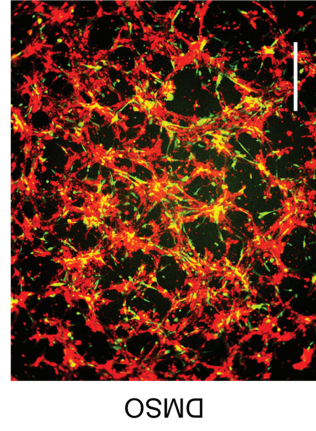
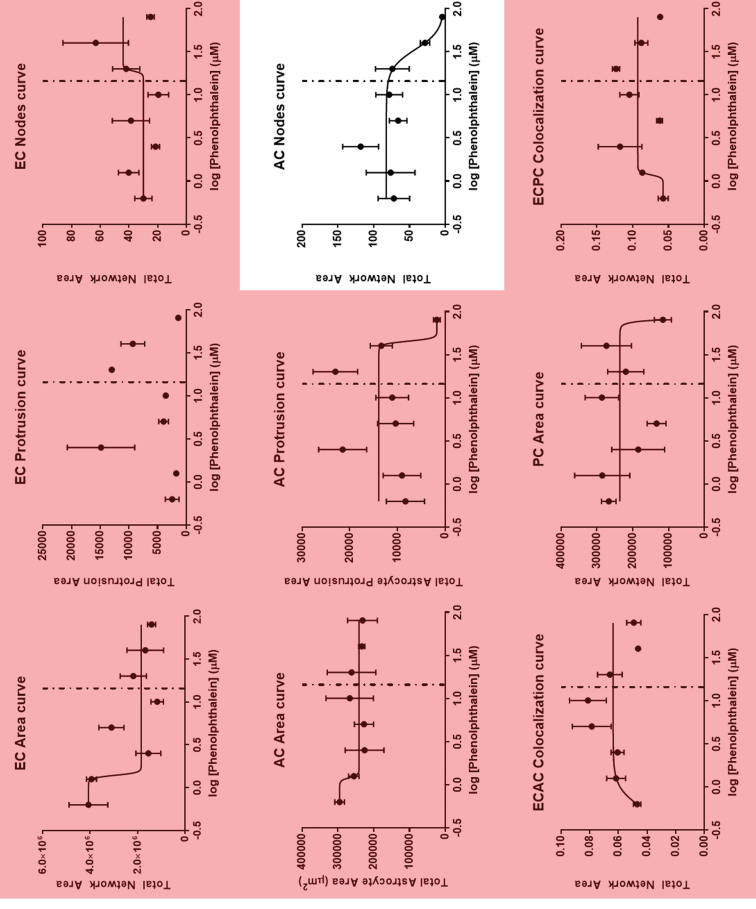
SUPPLEMENTARY FIG. S5. (Continued).

E

Phenolphthalein, PEG Hydrogel



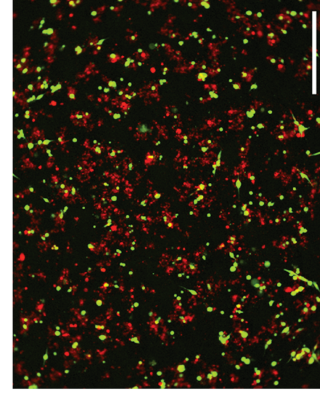
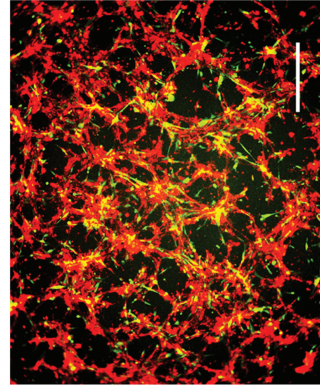
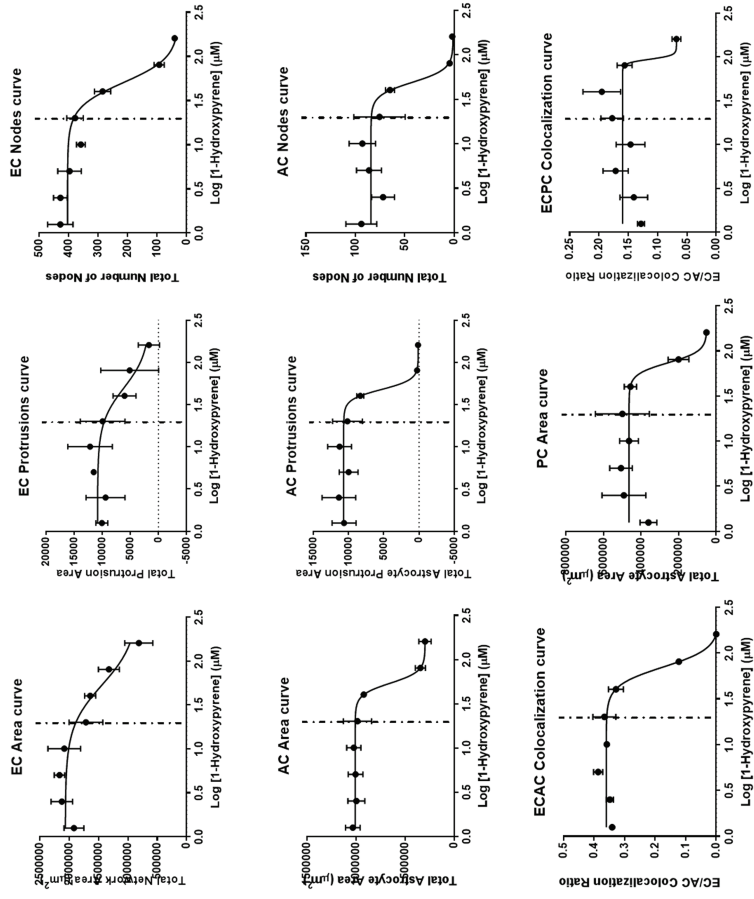
Phenolphthalein, Matrigel



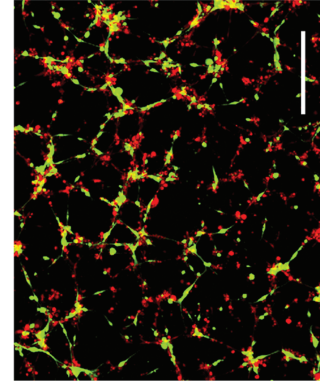
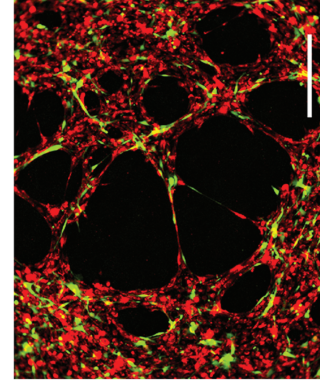
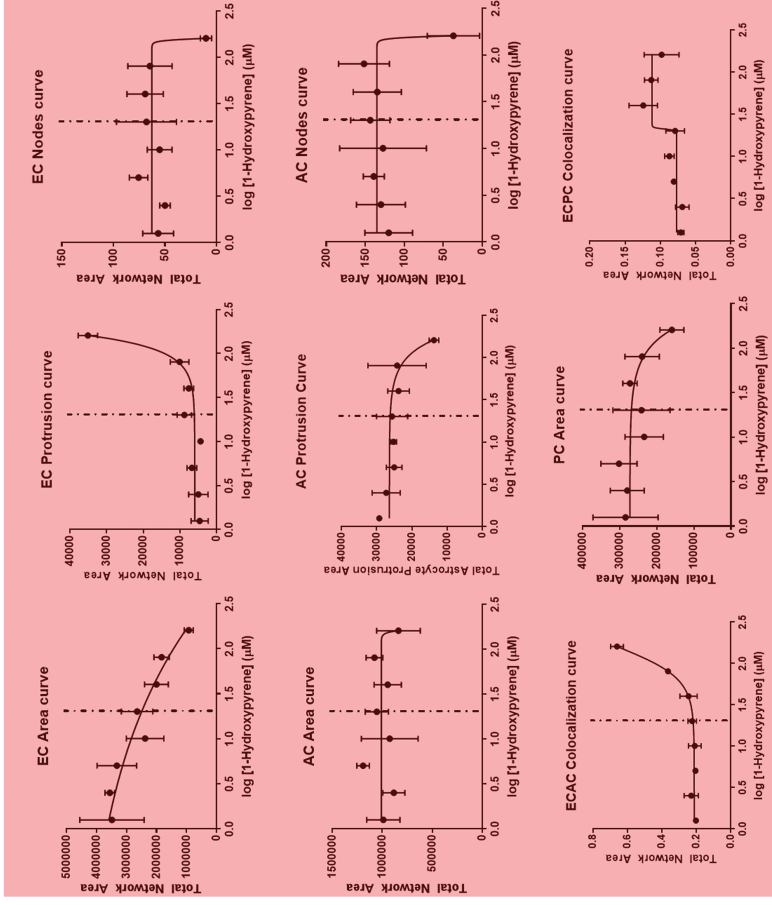
SUPPLEMENTARY FIG. S5. (Continued).

F

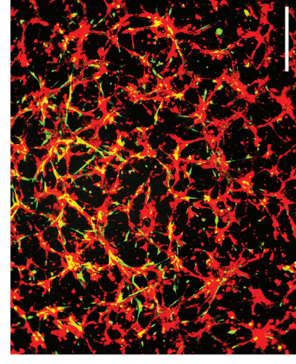
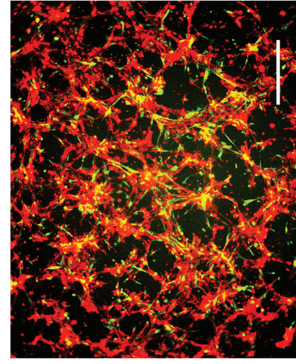
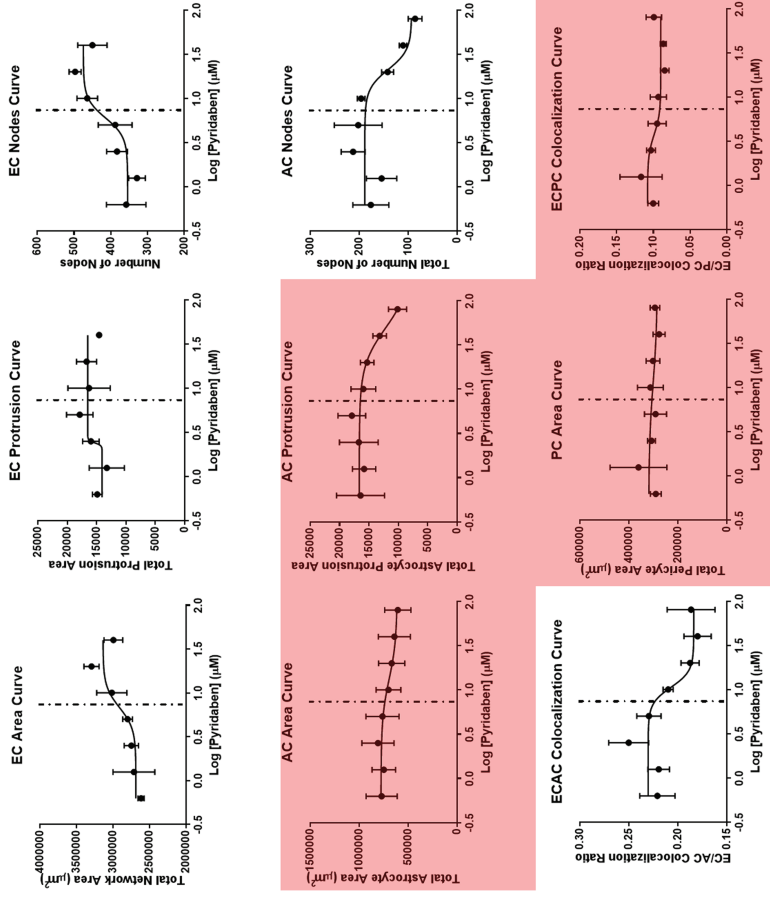
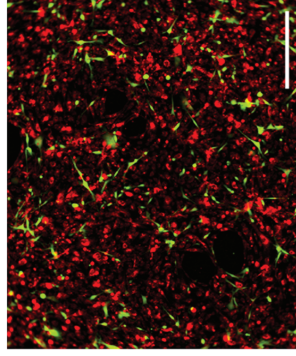
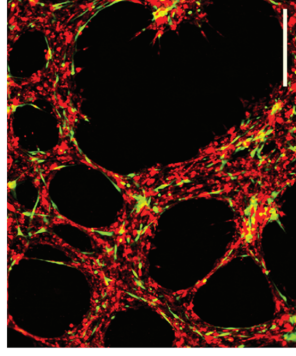
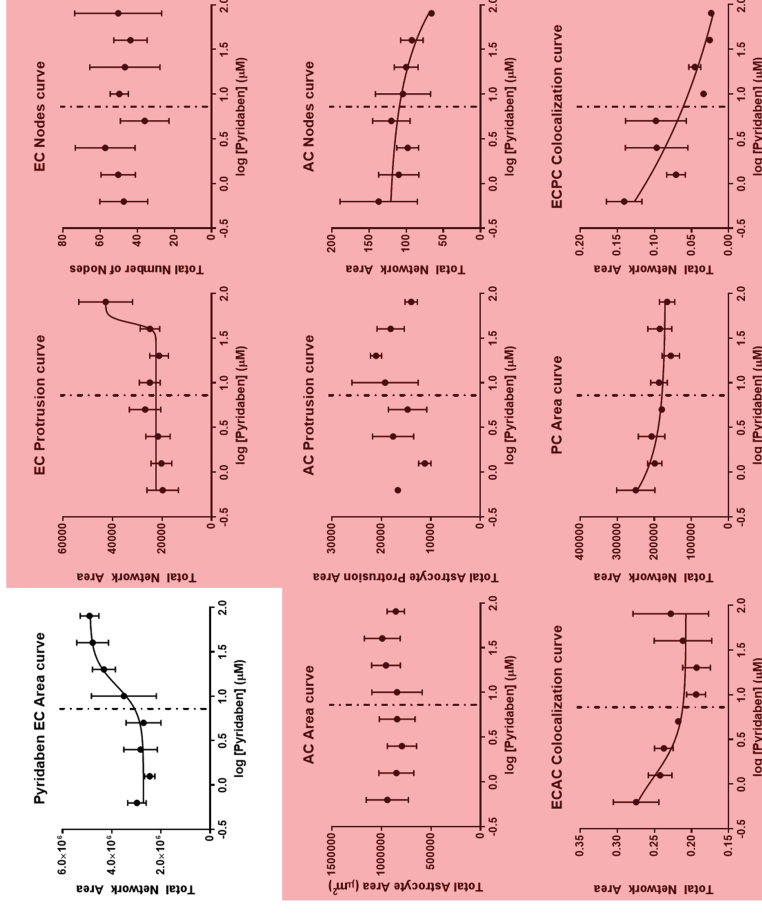
1-Hydroxypyrene, PEG Hydrogel

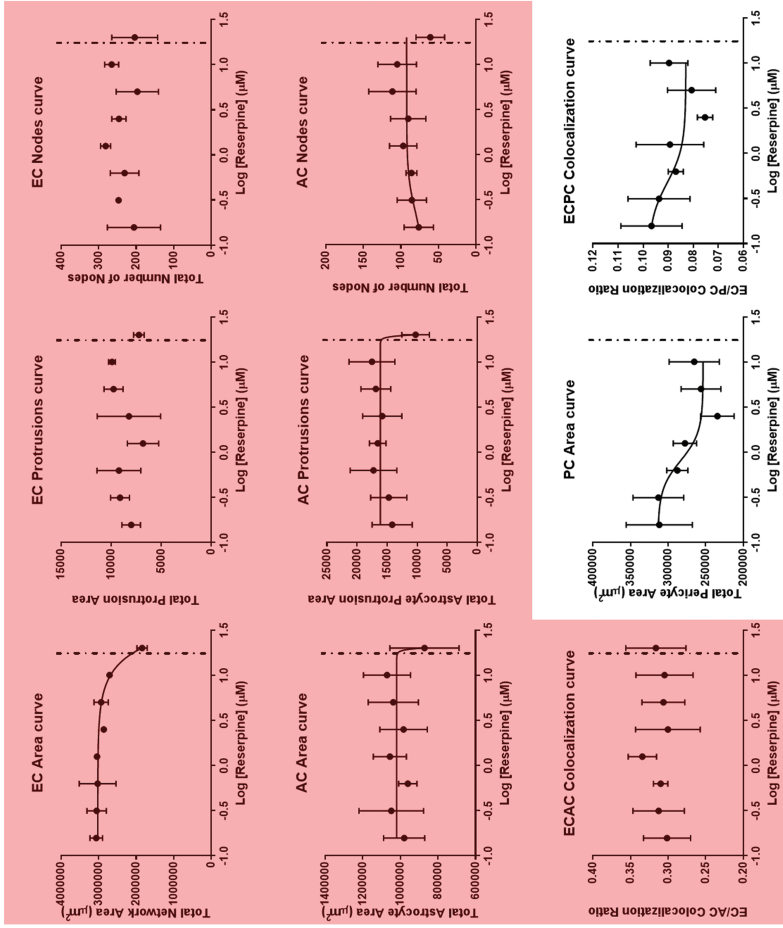
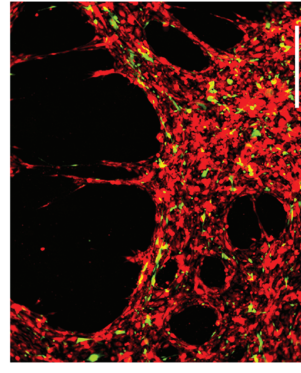
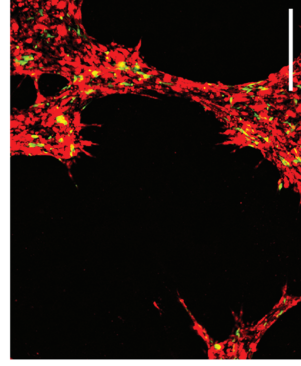
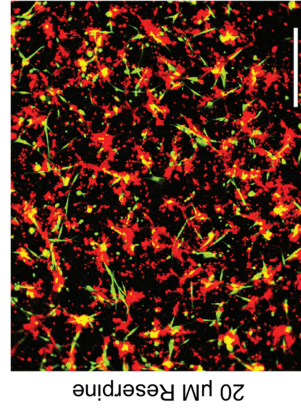
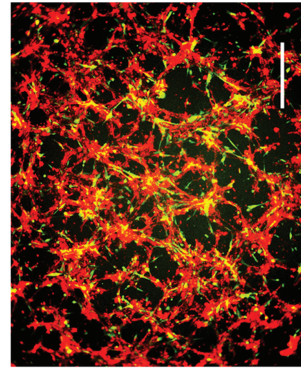
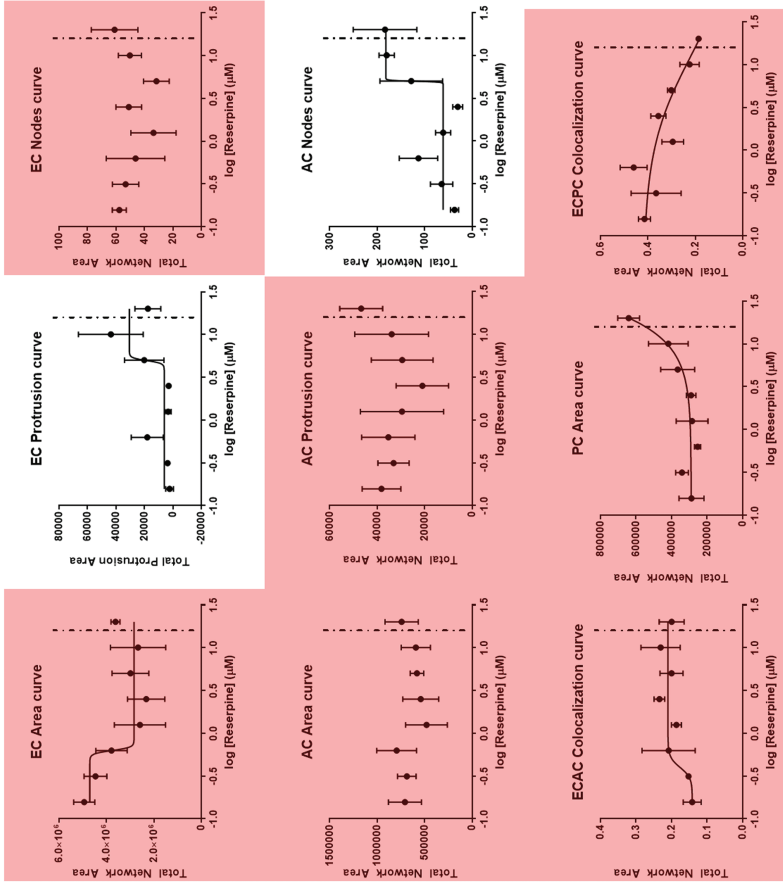


1-Hydroxypyrene, Matrigel

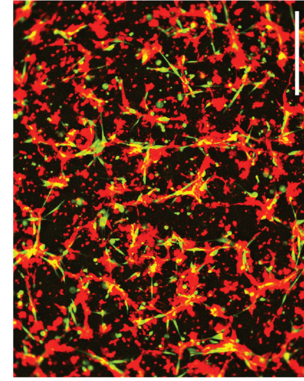
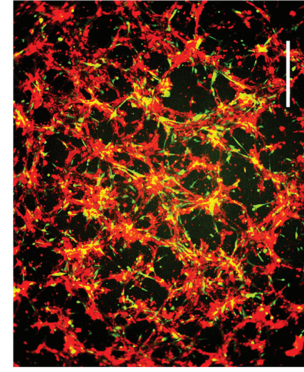
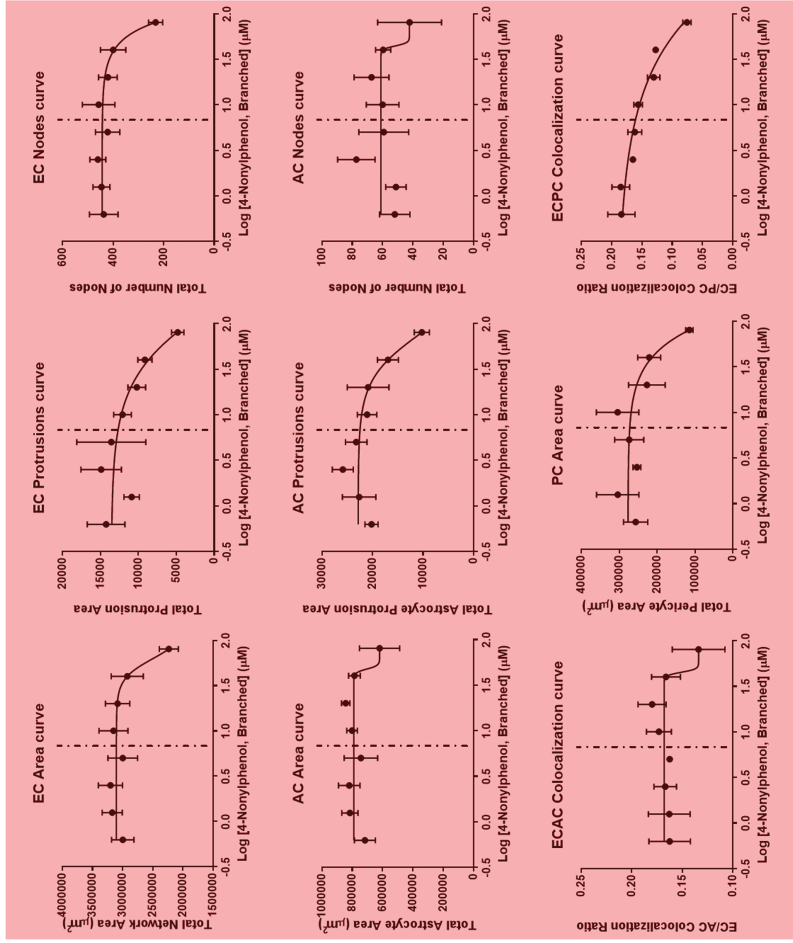


SUPPLEMENTARY FIG. S5. (Continued).

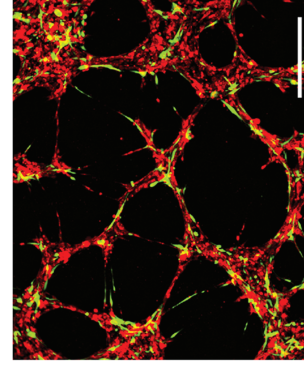
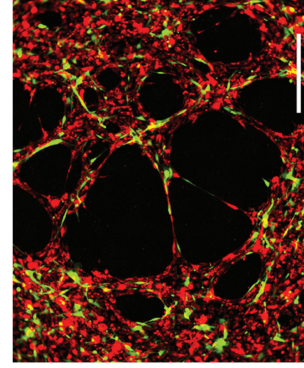
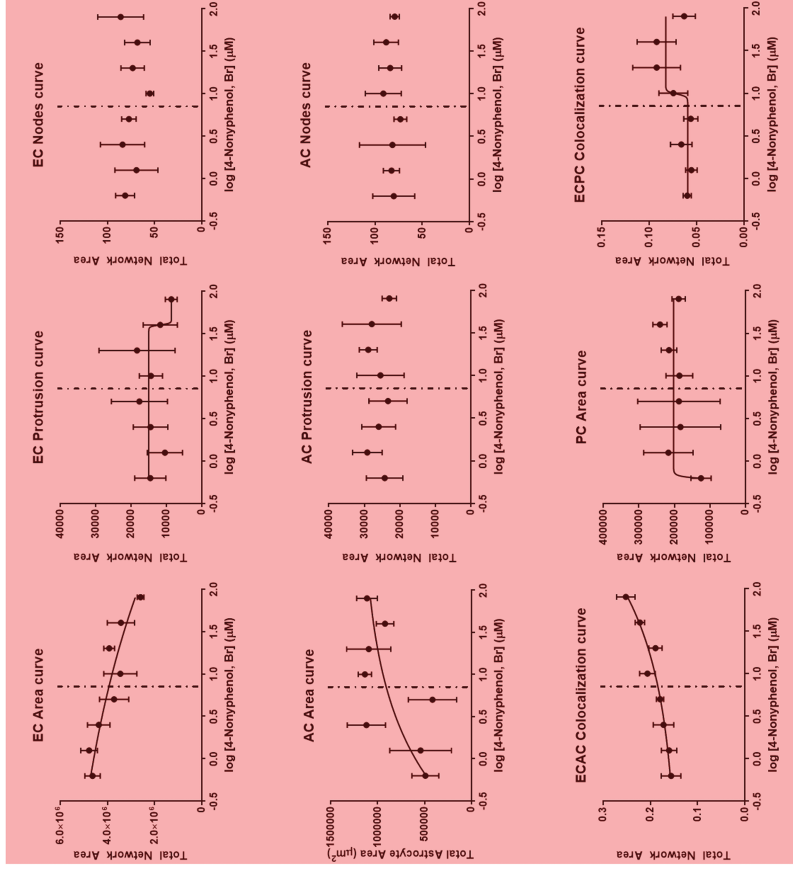
G**Pyridaben, PEG Hydrogel****Pyridaben, Matrigel****SUPPLEMENTARY FIG. S5. (Continued).**

H**Reserpine, PEG Hydrogel****Reserpine, Matrigel****SUPPLEMENTARY FIG. S5.** (Continued).

4 Nonylphenol, Branched, PEG Hydrogel



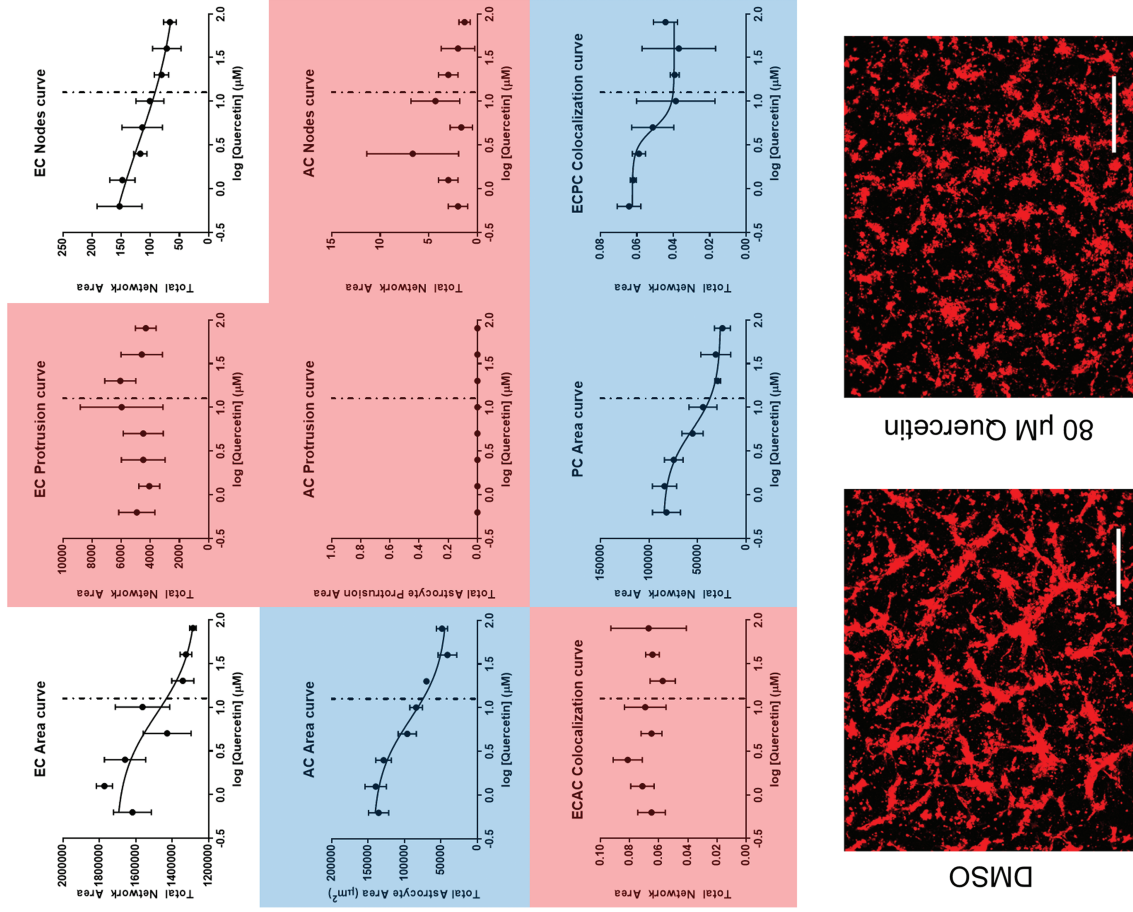
4 Nonylphenol, Branched, Matrigel



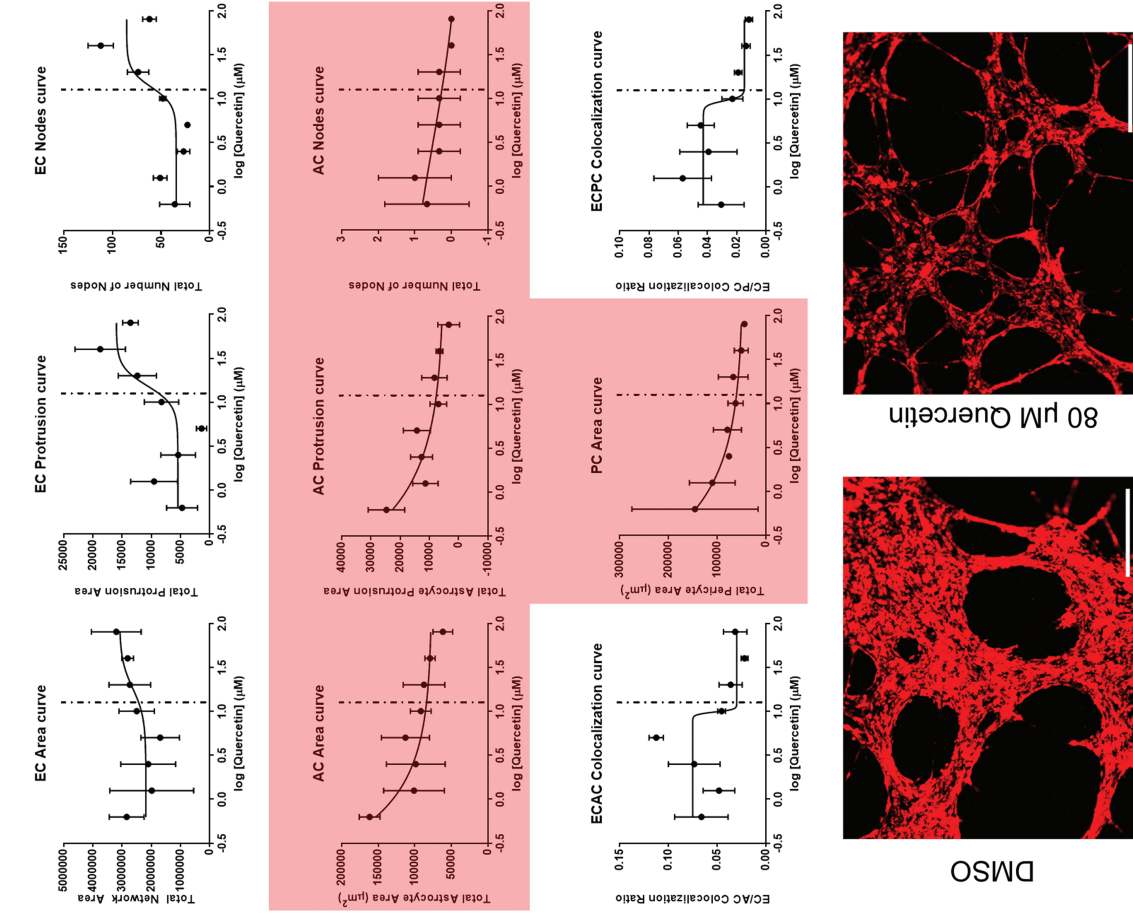
SUPPLEMENTARY FIG. S5. (Continued).

J

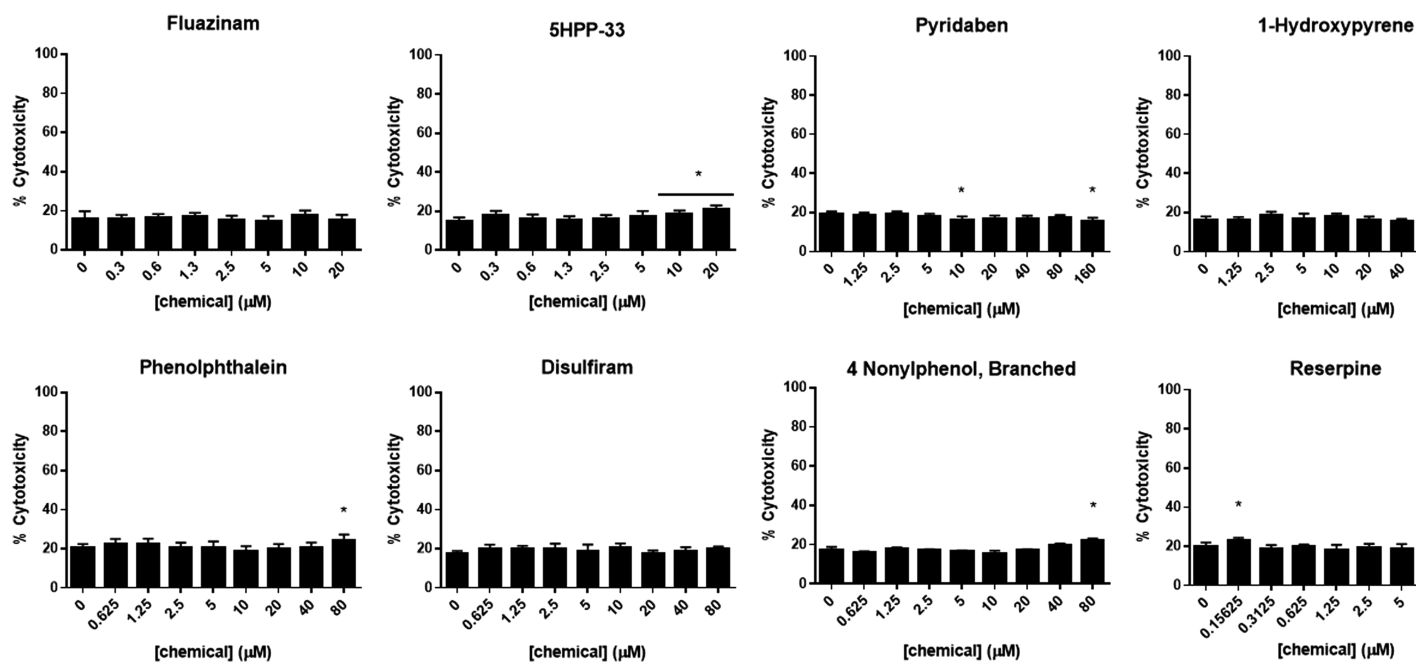
Quercetin, PEG Hydrogel



Quercetin, Matrigel



SUPPLEMENTARY FIG. S5. (Continued).



There is a possibility that the effectiveness of Matrigel in detecting disulfiram activity, but not fluazinam, phenolphthalein, and triclocarban, may highlight subtle differences in adverse outcome pathways between the four chemicals. These differences may be harder to detect using the PEG-based NVU model alone. Uniquely, 1-hydroxypyrene lost all ability to generate useful AC_{50} values on Matrigel. If the effect of 1-hydroxypyrene is a necrotic effect, the complex environment of Matrigel may dampen the effect. Pyridaben and quercetin largely affected EC morphology, and this was largely preserved between the NVU models. However, the visual effects of chemical exposure were distinct in the systems, likely due to the differential mechanisms of network formation on the materials.

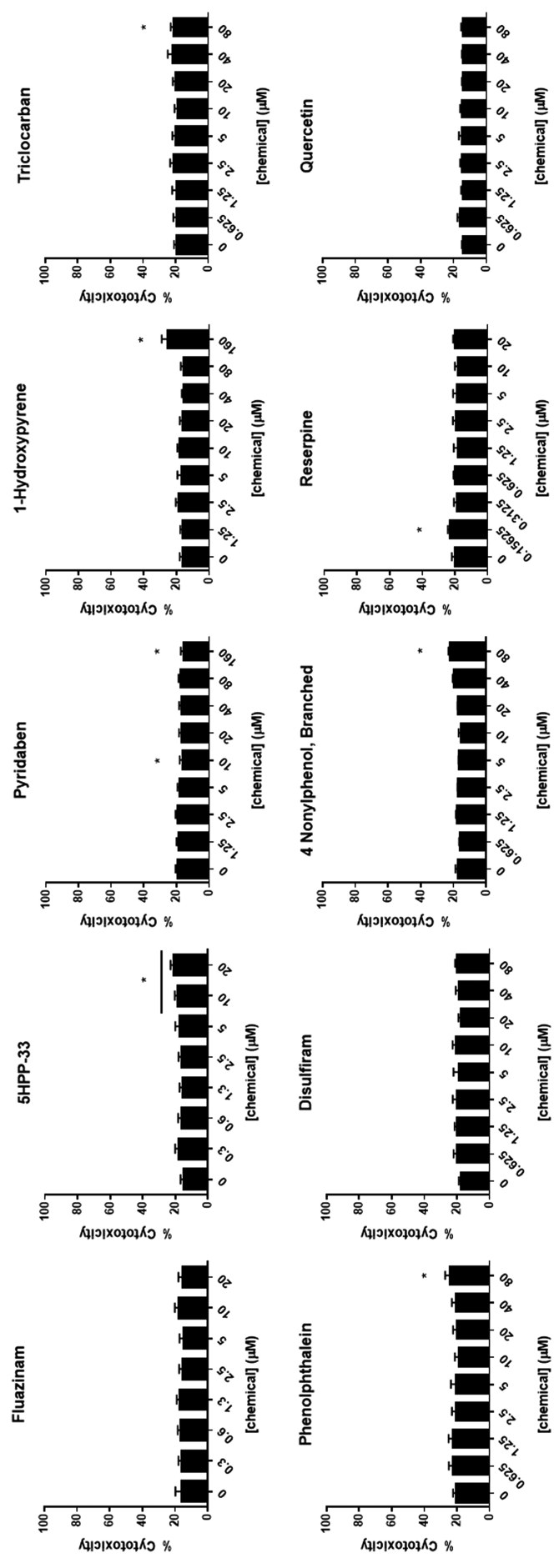
The final chemicals characterized with dose–response curves—reserpine and 4-nonylphenol branched—were not highly detectable in either NVU model. Although we did dose the chemicals in the recommended dose range, it may be possible that the neurotransmitter release mechanisms of reserpine^{S21,S22} or endocrine signaling mechanisms of 4-nonylphenol branched^{S23} may not be amenable to AC_{50} generation by either NVU model.

It should be noted that although most of the 10 chemicals studied here generated AC_{50} values that were within the range of AC_{50} values presented in the ToxCast library, 1-hydroxypyrene, reserpine, and 4-nonylphenol branched. This may occur through a combination of three possible reasons: (1) a novel mechanism of action is observable in our system, as may be the case with 1-hydroxypyrene’s necrotic effect, (2) the mechanism of action is related to a cell type not specifically tested in the ToxCast assays, as suggested by reserpine’s effects on PCs, or (3) the model was inappropriate to observing any relevant mechanisms of action of a given chemical, as suggested by the nonde-

tection of 4-nonylphenol branched. Results such as these highlight the need to develop numerous tissue toxicity models to gather information on chemical activity in a variety of biological contexts.

The 10 chemicals tested in this study were categorized by their ability to generate AC_{50} values specific to their related cell types: ECs, PCs, or ACs (Fig. 4E, Table 1). In general, the chemicals were either most effective in their ability to affect the cell types for which they were listed as “critical priority” or were effective at generating AC_{50} values for all cell types in the NVU model. The most effective chemicals in this case were pyridaben and phenolphthalein affecting ECs, and reserpine affecting PCs. The notable exception to this finding was 4-nonylphenol, branched, which failed to find AC_{50} values in our study. Regarding quercetin, it affected EC network properties strongly as predicted by the initial screens, but it also demonstrated autofluorescence effects that interfered with PC and AC measurements.

Any discrepancies that exist between the results of the initial screen and the AC_{50} curves could be related to the limited number of measurements used in the initial screen (EC area and colocalization measurements related to PCs and ACs only). In addition, although significant morphological changes were detected at 20 μ M chemical doses in the initial screen, this did not necessarily translate to the derivation of a full AC_{50} curve. Most of what is known about the activity of these chemicals on vasculature is found in the ToxCast database,^{S15} but novel findings related to specific effects on ECs, PCs, and ACs here can motivate more focused studies to determine mechanisms of action in these cell types. For example, although previous studies found that 10 μ M doses of disulfiram do not affect astrocyte proliferation,^{S8} the higher doses found in our studies (Table 1) affect other astrocyte properties that are potentially worth further characterization.



SUPPLEMENTARY FIG. S7. Cytotoxicity of tested chemicals on NVU models. Assays were performed using the Promega Cytotox[®] 96-well assay kit. Cytotoxicity, 100%, denotes LDH release in a lysis buffer control. * $p < 0.05$ compared with DMSO control, Dunnett's multiple comparison test. LDH, lactate dehydrogenase.

One limitation in the analysis used in these studies is autofluorescent interference by certain chemicals. This mainly concerned 5HPP33, reserpine, and quercetin. With 5HPP33 and reserpine, we were able to use lower concentrations of chemicals to generate functional dose–response curves if the autofluorescence levels began to interfere with PCs and ACs morphology analysis. Quercetin, an autofluorescent molecule often used to quantify cell uptake of flavonoids,^{S24} would likely result in false positives in screening experiments using epifluorescent microscopy. Quercetin clearly had antiangiogenic activity, as it was able to decrease total network area with increasing dose without impacting protrusions significantly. This was the only chemical able to do this, and is in agreement with suspected antiangiogenic capabilities of the chemical.^{S25,S26} However, PC and AC results were uncertain. We attempted to track PCs and ACs with Cell Tracker™ Blue to circumvent this issue, but blue autofluorescence levels in the PEG-based NVU model were proportional to quercetin present in the medium (Supplementary Fig. S5). Interestingly, this effect was not repeated on Matrigel, as all conditions had similar levels of autofluorescence in the presence of all tested concentrations of quercetin. This may suggest Matrigel’s superiority in performance with regard to dampening autofluorescence.

Additional limitations to this study should be addressed during further development of the PEG hydrogel-based screening system. A single induced pluripotent stem cell (iPSC) clone was used as a source of ECs and ACs in these studies, and each of these cells was expanded from a single lot. Future studies should evaluate the sensitivity of image analysis methods described here on cocultures derived from multiple iPSC clones to confirm data reproducibility.

It is also known that PCs require a period of time >24 hours to fully interact with neighboring cell types.^{S27} We have attempted to culture the NVU coculture for a period >24 hours, and we were able to preserve network structure for 72 hours (Supplementary Fig. S7) and through multiple media changes. However, by this time, desired throughput and fluorescent readouts were diminished, and proliferation levels began to exceed desired levels as well. This experiment does highlight the possibility for the assay to be adapted for longer term studies. However, in the context of conducting long-term toxicity studies, interactions between ECs, PCs, and ACs should be studied more closely, as many interactions may not manifest in the first 24 hours of culture.^{S27}

Finally, there is the potential to further improve the specificity and sensitivity of the screening assay. Rather than using a blanket criterion of a two-standard deviation change from means, we recommend that future iterations of the assay should tune the selection criteria based on the variability present in ECs, PCs, and ACs measurements.

Supplementary References

- S1. Fairbanks BD, Schwartz MP, Halevi AE, et al. A versatile synthetic extracellular matrix mimic via thiol-norbornene photopolymerization. *Adv Mater* 2009;21;5005–5010.
- S2. Roskoski R. Sunitinib: A VEGF and PDGF receptor protein kinase and angiogenesis inhibitor. *Biochem Biophys Res Commun* 2007;356:323–328.
- S3. Coyle CH, Martinez LJ, Coleman MC, et al. Mechanisms of H₂O₂-induced oxidative stress in endothelial cells. *Free Radic Biol Med* 2006;40:2206–2213.
- S4. Griendling KK, Sorescu D, Lassègue B, et al. Modulation of protein kinase activity and gene expression by reactive oxygen species and their role in vascular physiology and pathophysiology. *Arterioscler Thromb Vasc Biol* 2000;20:2175–2183.
- S5. Ong DB, Colley SM, Norman MR, et al. Transcriptional regulation of a BMP-6 promoter by estrogen receptor alpha. *J Bone Miner Res* 2004;19:447–454.
- S6. Hu JY, Aizawa T. Quantitative structure-activity relationships for estrogen receptor binding affinity of phenolic chemicals. *Water Res* 2003;37:1213–1222.
- S7. Ravdin PM, van Beurden M, Jordan VC. Estrogenic effects of phenolphthalein on human breast cancer cells in vitro. *Breast Cancer Res Treat* 1987;9:151–154.
- S8. Triscott J, Lee C, Hu K, et al. Disulfiram, a drug widely used to control alcoholism, suppresses the self-renewal of glioblastoma and over-rides resistance to temozolomide. *Oncotarget* 2012;3:1112–1123.
- S9. Kanbara Y, Murakane K, Nishimura Y, et al. Nanomolar concentration of triclocarban increases the vulnerability of rat thymocytes to oxidative stress. *J Toxicol Sci* 2013;38:49–55.
- S10. Han J, Won EJ, Hwang UK, et al. Triclosan (TCS) and triclocarban (TCC) cause lifespan reduction and reproductive impairment through oxidative stress-mediated expression of the defensome in the monogonont rotifer (*Brachionus koreanus*). *Comp Biochem Physiol C Toxicol Pharmacol* 2016;185–186:131–137.
- S11. Rashid A, Kuppa A, Kunwar A, et al. Thalidomide (5HPP-33) suppresses microtubule dynamics and depolymerizes the microtubule network by binding at the vinblastine binding site on tubulin. *Biochemistry* 2015;54:2149–2159.
- S12. Iguchi T, Yachide-Noguchi T, Hashimoto Y, et al. Novel tubulin-polymerization inhibitor derived from thalidomide directly induces apoptosis in human multiple myeloma cells: Possible anti-myeloma mechanism of thalidomide. *Int J Mol Med* 2008;21:163–168.
- S13. Li PK, Pandit B, Sackett DL, et al. A thalidomide analogue with in vitro antiproliferative, antimitotic, and microtubule-stabilizing activities. *Mol Cancer Ther* 2006;5:450–456.
- S14. Hecht SS, Carmella SG, Kotandeniya D, et al. Evaluation of toxicant and carcinogen metabolites in the urine of e-cigarette users versus cigarette smokers. *Nicotine Tob Res* 2015;17:704–709.
- S15. USEPA. ToxCast & Tox21 Summary Files from ToxCast Dashboard.
- S16. Yozzo KL, Isales GM, Raftery TD, et al. High-content screening assay for identification of chemicals impacting cardiovascular function in zebrafish embryos. *Environ Sci Technol* 2013;47:11302–11310.
- S17. Charli A, Jin H, Anantharam V, et al. Alterations in mitochondrial dynamics induced by tebufenpyrad and pyridaben in a dopaminergic neuronal cell culture model. *Neurotoxicology* 2016;53:302–313.
- S18. Lee JE, Kang JS, Shin IC, et al. Fluazinam-induced apoptosis of SH-SY5Y cells is mediated by p53 and Bcl-2 family proteins. *Neurotoxicology* 2011;32:702–710.
- S19. Lee JE, Kang JS, Ki YW, et al. Fluazinam targets mitochondrial complex I to induce reactive oxygen species-dependent cytotoxicity in SH-SY5Y cells. *Neurochem Int* 2012;60:773–781.

- S20. Padilla S, Corum D, Padnos B, et al. Zebrafish developmental screening of the ToxCast™ phase I chemical library. *Reprod Toxicol* 2012;33;174–187.
- S21. Saharia K, Arya U, Kumar R, et al. Reserpine modulates neurotransmitter release to extend lifespan and alleviate age-dependent A β proteotoxicity in *Caenorhabditis elegans*. *Exp Gerontol* 2012;47;188–197.
- S22. Mandela P, Chandley M, Xu YY, et al. Reserpine-induced reduction in norepinephrine transporter function requires catecholamine storage vesicles. *Neurochem Int* 2010;56;760–767.
- S23. Spagnoletti A, Paulesu L, Mannelli C, et al. Low concentrations of Bisphenol A and para-Nonylphenol affect extravillous pathway of human trophoblast cells. *Mol Cell Endocrinol* 2015;412;56–64.
- S24. Filippi A, Petrusa E, Peresson C, et al. In vivo assay to monitor flavonoid uptake across plant cell membranes. *FEBS Open Bio* 2015;5;748–752.
- S25. Jackson SJ, Venema RC. Quercetin inhibits eNOS, microtubule polymerization, and mitotic progression in bovine aortic endothelial cells. *J Nutr* 2006;136;1178–1184.
- S26. Ravishankar D, Watson KA, Boateng SY, et al. Exploring quercetin and luteolin derivatives as antiangiogenic agents. *Eur J Med Chem* 2015;97;259–274.
- S27. Al Ahmad A, Taboada CB, Gassmann M, et al. Astrocytes and pericytes differentially modulate blood-brain barrier characteristics during development and hypoxic insult. *J Cereb Blood Flow Metab* 2011;31;693–705.